Penerbit Akademia Baru

Journal of Advanced Research in Fluid Mechanics and Thermal Sciences
ISSN (online): 2289-7879 | Vol. 26, No. 1. Pages 1-19, 2016

Numerical Simulation and Analysis of Incompressible Newtonian Fluid Flows using FreeFem++

K. R. Mahmud [*,1], *M. M. Rhaman* [2] *and A. K. Al Azad* [1]

[1]Department of Computer Science and Engineering, Faculty of School of Science and Engineering, University of Liberal Arts Bangladesh, Dhaka-1209, Bangladesh.
[2]Department of Mathematics, Faculty of Science & Information Technology, American International University-Bangladesh, Dhaka-1213, Bangladesh.
[*]*raqib.mahmud@ulab.edu.bd*

Abstract –*We present the analysis and numerical simulations of incompressible Newtonian fluids for unsteady flows in a straight pipe and in deformed pipe with concave and convex deformation of the upper wall. An approach of modeling of blood flow is considered with an unsteady Navier-Stokes problem with a pulsatile flow for which we can establish analogy with existing cardio vascular systems. We apply the Finite Element Methods to obtain solutions and analyze the evolution of the flow over time. For the numerical simulations of fluid flows in complex geometries, FreeFem++ based on finite element method is used and we analyze the behavior of velocity and pressure qualitatively along time.*

Keywords: Navier-Stokes equations, Newtonian fluids, incompressible flows, pulsatile flow, finite element method, FreeFem++

1.0 INTRODUCTION

Incompressible Newtonian fluids flow is important to understand flow dynamics of biological fluids. This paper is mainly concerned with the analysis and numerical approximation of the nonstationary problem that models the motion of incompressible Newtonian fluids in different geometries. Given the complex behavior of this fluid, the second order partial differential governing equations are non-linear and they have the parabolic characteristic. The numerical simulations to unsteady Navier-Stokes equations were obtained computationally, by implementing the Finite Element Method [18].

Although there are several types of finite elements, we deal only with the discretization of the Navier-Stokes problem using a Lagrange Finite Element of type $P_2 - P_1$ for velocity and pressure respectively [5, 11, 18]. Through the application of the finite element method for the Navier-Stokes system, we present the results of numerical simulations and all results will be presented here for two-dimensional case.

The method Hood-Taylor is applied to the unsteady Navier-Stokes equations, and the corresponding linear system is solved by the direct method of Crout [10]. For this problem, we

Journal of Advanced Research in Fluid Mechanics and Thermal Sciences
ISSN (online): 2289-7879 | Vol. 26, No. 1. Pages 1-19, 2016

approach the evolution in time of the solution, following the method of Characteristics Galerkin. The choice of solver and validation of the numerical method was made by considering the problem of Kim-Moin in square domain $= [0.25, 1.25] \times [0.5, 1.5]$ for which it was considered for a refine mesh and a coarse mesh with several times steps [10].

All meshes and simulations were done in FreeFem++, the free software [7, 20] with its own high level programming language [17] based on the Finite Element Method to solve partial differential equations. FreeFem++ uses an automatic mesh generator based on Delaunay-Voronoi algorithm where the number of internal points is proportional to the number of points on the boundaries. We develop a programming code in FreeFem++ to find $(\mathbf{u}, p)$ using the variational formulation from the Navier-Stokes equations and use Crout method as a solver to solve the system. The direct numerical simulations from the variational formulation for the time discretization can be used, straightforwardly implemented on the FreeFem++.

From a wide range of applications of Newtonian fluids, we can mention in particular the behavior of blood in large arteries, since blood can be considered as a homogeneous and incompressible Newtonian fluid. For this reason, we have chosen some fictitious geometries similar to existent in some areas of cardio-vascular system [14] as well as geometries corresponding to pathological situations.

For the numerical simulations of the fluid flow we choose different case studies. As a first option we simulate the flow in a straight pipe whose boundary is made up of two rigid walls. Second option, we choose a pipe with deformation on the upper wall as analogy of the pathological situations in cardio vascular system. To simulate an abnormal narrowing of a blood vessel, usually called stenosis, we define the upper wall with a concave deformation. To simulate a dilation of the vascular wall, designated as aneurysm, we define a convex deformation on the upper wall. We present the qualitative behavior of normal and tangential velocity and the pressure inside these geometries. The motivation to consider of these cases is that similar types of real engineering problems are very prevalent [21, 22].

2.0 NAVIER-STOKES EQUATIONS AND FINITE ELEMENT APPROXIMATION

Let Ω is a bounded domain of $\mathbb{R}^d, d = 2,3$ with Lipschitz continuous boundary $\partial\Omega$. We use different function spaces with different notations details of which can be found in [1, 3, 15]. Without loss of generality, we consider an incompressible fluid confined into a domain with fixed boundary. Mathematically, for each $t \in [t_0, T]$ (to simplify, we take from now $t_0 = 0$), we write the unsteady Navier-Stokes equations with the Dirichlet boundary conditions $\mathbf{u} = \mathbf{g}$ on $\partial\Omega$ (adherence conditions). The condition $\mathbf{g} = 0$ is called the homogeneous Dirichlet boundary conditions (or no-slip boundary conditions) i.e., $\mathbf{u} = 0$ on $\partial\Omega$, which describes a fluid confined into a domain with fixed boundary (the boundary is at rest) [12, 16]. Given $\mathbf{f}$, find $(\mathbf{u}, p)$ such that

Penerbit Akademia Baru

Journal of Advanced Research in Fluid Mechanics and Thermal Sciences
ISSN (online): 2289-7879 | Vol. 26, No. 1. Pages 1-19, 2016

$$\begin{cases} \dfrac{\partial \mathbf{u}}{\partial t} + \mathbf{u}\cdot\nabla\mathbf{u} + \nabla p - \nu\Delta\mathbf{u} = \mathbf{f} \quad \text{in} \quad [0,T]\times\Omega, \\ \nabla\cdot\mathbf{u} = 0 \quad \text{in} \quad [0,T]\times\Omega, \\ \mathbf{u} = 0 \quad \text{on} \quad [0,T]\times\partial\Omega, \\ \mathbf{u}(t=0,\mathbf{x}) = \mathbf{u}_0(\mathbf{x}), \forall \mathbf{x}\in\Omega. \end{cases} \tag{1}$$

where $\mathbf{f}$ is a given external force field per unit mass, $\mathbf{u}$ is the velocity field, $\mathbf{u}_0$ is the known initial velocity field, p is the rate between the pressure and the density and ν is the constant kinematic viscosity.

The variational or weak formulation of Navier-Stokes equation consists of the integral equations over Ω obtained by integration, after multiplying the momentum equation and continuity equation by appropriate test functions. Let us suppose that $\mathbf{u}\in C^2([0,T]\times\overline{\Omega})$ and $p\in C^1([0,T]\times\overline{\Omega})$ are the classical (or strong) solution of (1). Consider two Hilbert spaces $\mathbf{V} = \mathbf{H}_0^1(\Omega)$ and $Q = L_0^2(\Omega)$ and take $\mathbf{v}\in\mathbf{V}$ and $q\in Q$ be two arbitrary test functions. Applying the Green's formula for the integration by parts and taking into account that $\mathbf{v}$ vanishes on the boundary and after simplifying we get the variational formulation of the Navier-Stokes problem as:

$\forall t\in[0,T]$, given $\mathbf{f}\in L^2(0,T;\mathbf{H}^{-1}(\Omega))$ and $\mathbf{u}_0\in\mathbf{H}_0^1(\Omega)$ with $\nabla\cdot\mathbf{u}_0 = 0$, find $(\mathbf{u}, p)\in L^2(0,T;\mathbf{V})\times L^2(0,T;Q)$ such that

$$\begin{cases} \displaystyle\int_\Omega \frac{\partial \mathbf{u}}{\partial t}\cdot\mathbf{v} + \int_\Omega (\mathbf{u}\cdot\nabla\mathbf{u}).\mathbf{v} - \int_\Omega p\nabla.\mathbf{v} + 2\nu\int_\Omega \mathbf{D}(\mathbf{u}):\mathbf{D}(\mathbf{v}) = \int_\Omega \mathbf{f}.\mathbf{v} \\ \displaystyle\int_\Omega q\nabla\cdot\mathbf{u} = 0 \\ \mathbf{u}(0) = \mathbf{u}_0 \end{cases} \tag{2}$$

for all $(\mathbf{v}, q)\in\mathbf{H}_0^1(\Omega)\times\mathbf{L}_0^2(\Omega)$. Here $\mathbf{D}(\mathbf{u}) = \frac{1}{2}(\nabla\mathbf{u} + (\nabla\mathbf{u})^T)$ is the deformation tensor. Taking into the definitions of the following bilinear and trilinear forms:

$a(\mathbf{u},\mathbf{v}) = 2\nu(\mathbf{D}(\mathbf{u}),\mathbf{D}(\mathbf{v})) = 2\nu\displaystyle\int_\Omega \mathbf{D}(\mathbf{u}):\mathbf{D}(\mathbf{v})$, $b(\mathbf{v}, p) = -(p,\nabla\cdot\mathbf{v}) = -\displaystyle\int_\Omega p\nabla\cdot\mathbf{v}$, and

$c(\mathbf{w},\mathbf{u},\mathbf{v}) = ((\mathbf{w}\cdot\nabla)\mathbf{u},\mathbf{v}) = \displaystyle\int_\Omega (\mathbf{w}\cdot\nabla)\mathbf{u}\cdot\mathbf{v}$

we can reformulate the variational formulation of the Navier-Stokes problem as follows:

$\forall t\in[0,T]$, given $\mathbf{f}\in L^2(0,T;\mathbf{H}^1(\Omega))$ and $\mathbf{u}_0\in\mathbf{H}_0^1(\Omega)$ with $\nabla\cdot\mathbf{u}_0 = 0$, find $(\mathbf{u}, p)\in L^2(0,T;\mathbf{V})\times L^2(0,T;Q)$ such that

Penerbit Akademia Baru
Journal of Advanced Research in Fluid Mechanics and Thermal Sciences
ISSN (online): 2289-7879 | Vol. 26, No. 1. Pages 1-19, 2016

$$\begin{cases} (\frac{\partial \mathbf{u}}{\partial t}, \mathbf{v}) + a(\mathbf{u}, \mathbf{v}) + c(\mathbf{u}, \mathbf{u}, \mathbf{v}) + b(\mathbf{v}, p) = (\mathbf{f}, \mathbf{v}) \\ b(\mathbf{u}, q) = 0 \\ \mathbf{u}(0) = \mathbf{u}_0 \end{cases} \tag{3}$$

for all $(\mathbf{v}, q) \in \mathbf{H}_0^1(\Omega) \times L_0^2(\Omega)$.

It can be proved [9] that the problem (3) is well posed and equivalent to (1). The existence and uniqueness of theorem for the solutions of Navier-Stokes system can be found in [4-6, 9].

We consider finite element method (FEM) [18] to approximate the numerical solutions of Navier-Stokes problem (3). The FEM is a method which approaches the solution of partial differential equations (PDEs) and is a general technique for constructing approximate solutions to boundary value problems in dimension $d, (d \leq 3)$. All results will be presented here for the two-dimensional case, where we will do the application of these concepts and presentation of numerical simulations. Although there are several types of finite elements, in the following, we deal only with the discretization of the Navier-Stokes problem, using a Lagrange Finite Element of type $P_2 - P_1$.The solution $(\mathbf{u}, p)$ of the problem (3) lives in a space of infinite dimension. In this circumstance, it is generally impossible to calculate the exact solution. Then we determine an approximation of $\mathbf{u}$ and p, respectively $\mathbf{u}_h$ and p_h, each one defined in finite dimensional appropriate spaces V_h, such that $\dim V_h = I(h) (\lim_{h \to 0} I(h) = +\infty)$ and dependent on a parameter $h > 0$. These spaces are formed by polynomials and for all function v_h in V_h (in particular $\mathbf{u}_h$ and p_h for the appropriate spaces) we have

$v_h = \sum_{i=1}^{I} \alpha_i \varphi_i, \alpha \in IR, i = 1, \cdots, I$, where $\{\varphi_1, \varphi_2, \cdots, \varphi_I\}$ is a basis of V_h.

This is the principle of the Finite Element Method. The FEM can be studied in details in [2, 6, 8, 11]. We use classical Galerkin method to find the solution. We consider Galerkin's method for constructing approximate solutions to the variational boundary-value problem (2) or its abstract formulation (3). Galerkin's method consists of seeking an approximate solution (2) in a finite-dimensional subspace V_h of the space of admissible functions where the solution lies in this subspace rather than in the whole space. The natural Galerkin approximation for problem (1) is a mixed method which is based on Lagrange multiplier formulations of constrained problems. We refer to mixed approximation methods as those associated to the approximation of saddle point problems, in which there are two bilinear forms and two approximation spaces satisfying a compatibility condition known as the discrete LBB (or inf-sup) condition [8, 19] which reads as follows:

There exists $\beta > 0 (\text{independent of } h)$ such that $\inf_{q_h \in Q_h \setminus \{0\}} \sup_{v_h \in V_h^0 \setminus \{0\}} \frac{|(q_h, \nabla . v_h)|}{\left\| v_h \right\| \left| v_h^0 \right| \left\| q_h \right\|_{Q_h}} \geq \beta$

Penerbit Akademia Baru

Journal of Advanced Research in Fluid Mechanics and Thermal Sciences
ISSN (online): 2289-7879 | Vol. 26, No. 1. Pages 1-19, 2016

Let $\{T_h\}_{h>0}$ be a family of triangulations and h denotes a discretization parameter and let $\mathbf{V}_h$ and Q_h be two finite dimensional spaces such that $\mathbf{V}_h \in \mathbf{H}^1(\Omega)$ and $Q_h \in L^2(\Omega)$. We let $\mathbf{V}_h^0 := \mathbf{V}_h \cap \mathbf{H}_0^1(\Omega)$ and $M_h := Q_h \cap L_0^2(\Omega)$.

In these spaces, the discrete finite element approximation problem of (3) can be written as follows:

for each $t \in [0,T]$, $\mathbf{u}_{0,h} \in \mathbf{V}_h^0$, find $(\mathbf{u}_h, p_h) \equiv (\mathbf{u}_h(t,\cdot), p_h(t,\cdot)) \in \mathbf{V}_h^0 \times M_h$ such that

$$\begin{cases} \dfrac{d}{dt}(\mathbf{u}_h, \mathbf{v}_h) + a(\mathbf{u}_h, \mathbf{v}_h) + c(\mathbf{u}_h, \mathbf{u}_h, \mathbf{v}_h) + b(\mathbf{v}_h, p_h) = (\mathbf{f}, \mathbf{v}_h) \quad \forall \mathbf{v}_h \in \mathbf{V}_h^0, \\ b(\mathbf{u}_h, q_h) = 0 \qquad \forall q_h \in M_h, \\ \mathbf{u}_h(0) = \mathbf{u}_{0,h} \end{cases} \tag{4}$$

which can be written as for each $t \in [0,T]$, $\mathbf{u}_{0,h} \in \mathbf{V}_h^0$, find $(\mathbf{u}_h, p_h) \equiv (\mathbf{u}_h(t,\cdot), p_h(t,\cdot)) \in \mathbf{V}_h^0 \times M_h$ such that

$$\begin{cases} \int_\Omega \dfrac{\partial \mathbf{u}_h}{\partial t} \cdot \mathbf{v}_h + \int_\Omega (\mathbf{u}_h \cdot \nabla \mathbf{u}_h).\mathbf{v}_h - \int_\Omega p_h \nabla.\mathbf{v}_h + 2\nu \int_\Omega \mathbf{D}(\mathbf{u}_h) : \mathbf{D}(\mathbf{v}_h) = \int_\Omega \mathbf{f}.\mathbf{v}_h \qquad \forall \mathbf{v}_h \in \mathbf{V}_h^0 \\ \int_\Omega q_h \nabla \cdot \mathbf{u}_h = 0 \qquad \forall q_h \in M_h \\ \mathbf{u}_h(0) = \mathbf{u}_{0,h} \end{cases} \tag{5}$$

As motion is non-stationary we need to discretize the Navier-Stokes equations over time. There are several methods of time discretization. In this paper we use Characteristic Galerkin Method which associates backward Euler scheme of first order defined by

$$\frac{\partial \boldsymbol{u}}{\partial t}(t^{n+1},.) = \frac{\boldsymbol{u}(t^{n+1},.) - \boldsymbol{u}(t^n,.)}{t^{n+1} - t^n}$$

The Characteristic Galerkin Method evaluates time derivatives of vector field on Lagrangian frame, appealing to characteristic lines or trajectories described by a material particle when it has been driven by the field at the velocity of the field. We describe the motion of material particle of Newtonian fluid during the time interval $[t_0, t_1] \subset [0,T], (T > 0)$, which was in position ξ at instant t_o by

$$\chi_{t;t_0} : \xi \to \chi(t; t_0, \xi)$$

and define its characteristics line or trajectory, with the same flow direction, by the only solution of Cauchy problem

$$\begin{cases} \dfrac{d\chi}{dt}(t; t_0, \xi) = \boldsymbol{u}\big(t; \chi(t; t_0, \xi)\big), t \in]0,T[\\ \chi(t_0; t_0, \xi) = \xi \end{cases}$$

Now taking an uniform mesh of [0,T] defined by $t^n = n\Delta t, n = 0, \ldots, \frac{T}{\Delta t}$, Δt being the time step and applying the backward Euler scheme we can write the scheme for the problem (1), denoting $\boldsymbol{u}^n o \chi^n(\boldsymbol{x}) \approx \boldsymbol{u}^n\big(\boldsymbol{x} - \Delta t \mathbf{u}(\mathrm{t}^{n+1}, \mathbf{x})\big) = \mathbf{u}^{\mathrm{n}}(\mathbf{x}^*)$

Penerbit Akademia Baru

Journal of Advanced Research in Fluid Mechanics and Thermal Sciences
ISSN (online): 2289-7879 | Vol. 26, No. 1. Pages 1-19, 2016

$$\begin{cases} \boldsymbol{u}^{n+1} + \Delta t \nabla p^{n+1} - 2\nu\Delta t \nabla . \mathbf{D}(\boldsymbol{u}^{n+1}) = \Delta t \boldsymbol{f}^{n+1} + \mathbf{u}^{n}(\mathbf{x}^{*}), \\ \nabla . \mathbf{u}^{n+1} = 0, \\ \mathbf{u}^{n+1} = 0, \ \mathbf{u}^{0} = \mathbf{u}_{0} \end{cases} \tag{6}$$

The discrete variational formulation of (6) is as follows:

for each $t^{n+1} = (n+1)\Delta t \in [0,T]$, $(n \in \mathbf{N}_0)$ given $\mathbf{u}_h^0 = \mathbf{u}_h(0)$, find $(\mathbf{u}_h^{n+1},\ p_h^{n+1}) \in \mathbf{V}_h^0 \times M_h$ such that

$$\begin{cases} (\mathbf{u}_h^{n+1}, \mathbf{v}_h) - \Delta t(p_h^{n+1}, \nabla \cdot \mathbf{v}_h) + 2\nu\Delta t(\mathbf{D}(\mathbf{u}_h^{n+1}), \mathbf{D}(\mathbf{v}_h)) = (\mathbf{g}, \mathbf{v}_h) \quad in\ \Omega, \\ (\nabla \cdot \mathbf{u}_h^{n+1}, p_h^{n+1}) = 0 \quad in \quad \Omega. \end{cases} \tag{7}$$

where $\mathbf{g}^{n+1} = \Delta t \mathbf{f}^{n+1} + \mathbf{u}^{n}(\mathbf{x}^{*})$.

Let $\{\varphi_i\}_{i=1,\cdots,N_h}$ and $\{\psi_j\}_{j=1,\cdots,m_h}$ be the Lagrange bases of the spaces $\mathbf{V}_h^0$ and M_h respectively. Given $\mathbf{u}_h^n$, we express the corresponding approximate solutions $\mathbf{u}_h^{n+1} = (u_{1,h}^{n+1}, u_{2,h}^{n+1})$ and p_h^{n+1} in the basis of $\mathbf{V}_h^0$ and M_h

$u_{1,h}^{n+1} = \sum_{j=1}^{N_h} u_{1,j}^{n+1} \varphi_j$, $u_{2,h}^{n+1} = \sum_{j=1}^{N_h} u_{2,j}^{n+1} \varphi_j$, $p_h^{n+1} = \sum_{k=1}^{m_h} p_k^{n+1} \psi_k$ and with the test functions $\varphi_i \in \mathbf{V}_h^0$ and $\psi_k \in M_h$, we obtain the following linear algebraic system [13] in matrical form as:

$$\begin{bmatrix} \mathbf{A}_1 & \mathbf{A}_2 & \mathbf{B}_x \\ \mathbf{A}_2^t & \mathbf{A}_1 & \mathbf{B}_y \\ \mathbf{B}_x^t & \mathbf{B}_y^t & 0 \end{bmatrix} \begin{bmatrix} u_1^{n+1} \\ u_2^{n+1} \\ p^{n+1} \end{bmatrix} = \begin{bmatrix} \mathbf{b}_1 \\ \mathbf{b}_2 \\ 0 \end{bmatrix} \tag{8}$$

where $\mathbf{u}_k^{n+1} = \left[u_{k,1}^{n+1}, \cdots, u_{k,N_h}^{n+1}\right]^t$ and $p^{n+1} = \left[p_1^{n+1}, \cdots, p_{m_h}^{n+1}\right]^t$ are the vectors of unknown degree of freedom and

$$\mathbf{A}_1 = \left[\mathbf{A}_{1ij}\right]_{N_h \times N_h} = \left[\int_\Omega \left[\varphi_i \varphi_j + \nu\Delta t\left(2\frac{\partial \varphi_i}{\partial x}\frac{\partial \varphi_j}{\partial x} + \frac{\partial \varphi_i}{\partial y}\frac{\partial \varphi_j}{\partial y}\right)\right]\right]_{N_h \times N_h}$$

$$\mathbf{A}_2 = \left[\mathbf{A}_{2ij}\right]_{N_h \times N_h} = \left[\int_\Omega \frac{\partial \varphi_i}{\partial x}\frac{\partial \varphi_j}{\partial y}\right]_{N_h \times N_h} \quad \mathbf{B}_x = \left[\mathbf{B}_{xjk}\right]_{N_h \times m_h} = \left[-\int_\Omega \frac{\partial \varphi_i}{\partial x}\psi_k\right]_{N_h \times m_h}$$

$$\mathbf{B}_y = \left[\mathbf{B}_{yjk}\right]_{N_h \times m_h} = \left[-\int_\Omega \frac{\partial \varphi_i}{\partial y}\psi_k\right]_{N_h \times m_h} \quad \mathbf{b}_i = \left[\int_\Omega \mathbf{g}_{i,j}^{n+1}\varphi_i\right]_{N_h \times 1}$$

We can rewrite the above matrical equation in a simpler way

$$\begin{bmatrix} \mathbf{A} & \mathbf{B} \\ \mathbf{B}^t & 0 \end{bmatrix} \begin{bmatrix} \mathbf{u} \\ p \end{bmatrix} = \begin{bmatrix} \mathbf{b} \\ 0 \end{bmatrix} \text{ with } \mathbf{A} = \begin{bmatrix} \mathbf{A}_1 & \mathbf{A}_2 \\ \mathbf{A}_2^t & \mathbf{A}_1 \end{bmatrix},\ \mathbf{B} = \begin{bmatrix} \mathbf{B}^x \\ \mathbf{B}^y \end{bmatrix},\ \mathbf{u} = \begin{bmatrix} u_1 \\ u_2 \end{bmatrix} \text{ and } \mathbf{b} = \begin{bmatrix} b_1 \\ b_2 \end{bmatrix}$$

Penerbit Akademia Baru

Journal of Advanced Research in Fluid Mechanics and Thermal Sciences
ISSN (online): 2289-7879 | Vol. 26, No. 1. Pages 1-19, 2016

3.0 MATHEMATICAL MODELING AND IMPLEMENTATION OF BOUNDARY CONDITION

With the aim of modeling the blood flow we consider the fluid confined in a domain with upper and lower boundary as rigid walls denoted by Γ^w , an upstream section S_1 and downstream section S_2 through which the fluid enters and leaves Ω respectively. An inflow parabolic profile with respect to time is prescribed on upstream section, while on downstream section homogeneous Neumann conditions are assigned S_1 and S_2 are fictitious boundaries, since the vascular system is closed and there is no such boundary. We also assume that the flow tends smoothly to equilibrium as $t \to +\infty$, which mathematically translated by $f = 0$. Combined form of above boundary conditions can be provided as follows:

$$\begin{cases} \mathrm{u} = 0 & \text{on } \Gamma^w \\ \mathrm{T.n} = \sigma n = -\dfrac{P_{in}}{2}\left[1 - \cos\left(\dfrac{\pi t}{2.5}\right)\right] & \text{on } S_1 \\ \mathrm{T.n} = 0 & \text{on } \mathrm{S}_2 \end{cases} \tag{9}$$

T being the Cauchy stress tensor. The first condition of (9) guarantees the perfect adherence of the fluid to the wall while the second stages of the fluid enter with a pressure given by $-\dfrac{P_{in}}{2}\left[1 - \cos\left(\dfrac{\pi t}{2.5}\right)\right]$ and the last indicates that there is no normal reaction over the boundary. We suppose that the fluid is initially at rest, although some time-varying transition should be expected before reaching the time-periodic regime, the main characteristics of the flow patterns are presented even when starting the simulation from the at-rest state. The input profile $\mathbf{T} \cdot \mathbf{n}$ on S_1 is shown in Fig. 3.1

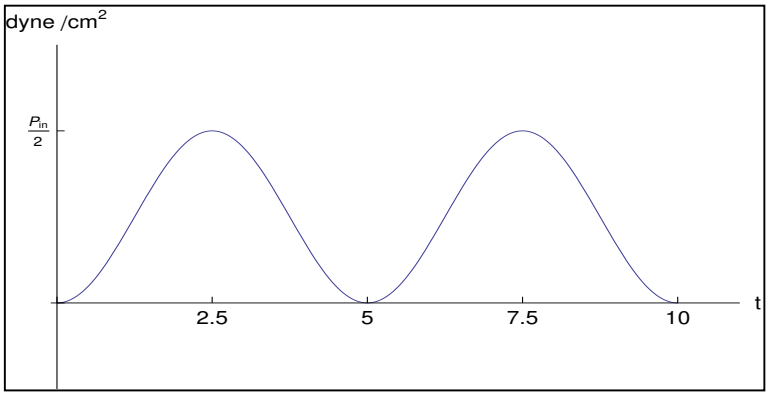

Figure 3.1: The input profile of inflow Neumann boundary condition.

Taking the test function $v \in V = \left\{v \in \mathbf{H}^1(\Omega) : v = 0 \; on \; \Gamma^w\right\}$ and applying the Green's formula results

$$\int_\Omega \frac{\partial \mathbf{u}}{\partial t} \cdot \mathbf{v} + \int_\Omega (\mathbf{u} \cdot \nabla)\mathbf{u}.\mathbf{v} - \int_\Omega p \nabla.\mathbf{v} + 2\nu \int_\Omega \mathbf{D}(\mathbf{u}) : \mathbf{D}(\mathbf{v}) - \int_{\partial\Omega} \mathbf{T}.\mathbf{n}.v = 0$$

Penerbit Akademia Baru
Journal of Advanced Research in Fluid Mechanics and Thermal Sciences
ISSN (online): 2289-7879 | Vol. 26, No. 1. Pages 1-19, 2016

$$\Leftrightarrow \int_{\Omega} \frac{\partial \mathbf{u}}{\partial t} \cdot \mathbf{v} + \int_{\Omega} (\mathbf{u} \cdot \nabla)\mathbf{u}.\mathbf{v} - \int_{\Omega} p \nabla.\mathbf{v} + 2\nu \int_{\Omega} \mathbf{D}(\mathbf{u}) : \mathbf{D}(\mathbf{v}) = \int_{\partial\Omega} \sigma n .v$$

So, the discrete variational problem of Navier-Stokes equations with boundary condition as follows:

Find $(\mathbf{u}, p) \in L^2(0,T;V) \times L^2(0,T;Q)$ with $\mathbf{u}(0,x) = 0, \forall x \in \Omega$ such that :

$$\begin{cases} \int_{\Omega} \frac{\partial \mathbf{u}}{\partial t} \cdot \mathbf{v} + \int_{\Omega} (\mathbf{u} \cdot \nabla)\mathbf{u}.\mathbf{v} - \int_{\Omega} p \nabla.\mathbf{v} + 2\nu \int_{\Omega} \mathbf{D}(\mathbf{u}) : \mathbf{D}(\mathbf{v}) = \int_{\partial\Omega} \sigma n .v, \ \forall \mathbf{v} \in \mathbf{V} \\ \int_{\partial\Omega} \mathbf{u} .q = 0 \qquad\qquad \forall q \in Q \end{cases}$$

We obtain the following discretized problem:

for each $t^{n+1} \in [0,T]$, find $(\mathrm{u}_{\mathrm{h}}^{\mathrm{n+1}}, p_h^{n+1}) \in V_h^0 \times M_h^0$ such that :

$$\begin{cases} \int_{\Omega} u_h^{n+1} \cdot \mathbf{v}_h - \Delta t \int_{\Omega} p_h^{n+1} \nabla.\mathbf{v}_h + 2\nu\Delta t \int_{\Omega} \mathbf{D}(\mathbf{u}_h^{n+1}) : \mathbf{D}(\mathbf{v}_h) + \frac{\Delta t}{2} \int_{\Omega} (\nabla.u_h^n) u_h^{n+1}.v_h \\ \qquad = \int_{S_1} -\frac{P_{in}}{2}\left[1 - \cos\left(\frac{\pi t}{2.5}\right)\right].n.v_h \qquad \forall \mathbf{v}_h \in \mathbf{V}_h^0 \\ \int_{\partial\Omega} u_h^{n+1} . q_h = 0 \qquad\qquad \forall q \in Q \\ u_h(0) = 0 \qquad \text{on } \Gamma^w \end{cases}$$

Given Δt, for each $t^{n+1} = (n+1)\Delta t, \left(n = 0,1,\ldots,\frac{T}{\Delta t}\right)$, we take $\mathrm{u}_{1,\mathrm{h}}^{\mathrm{n+1}}, \mathrm{u}_{2,\mathrm{h}}^{\mathrm{n+1}}$ and $\mathrm{p}_{\mathrm{h}}^{\mathrm{n+1}}$, we obtain a system with:

$$b_1 = \left[\int_{S_1} -\frac{P_{in}}{2}\left[1 - \cos\left(\frac{\pi t}{2.5}\right)\right].n\varphi_i.\right]_{N_h \times 1}$$

4.0 FLOWS IN A STRAIGHT PIPE

To analyze the flow in a straight pipe we consider the propagation of a Newtonian fluid in a straight pipe of length $L = 6$ by imposition of two fictitious borders $S_1 = \{0\} \times [0,1]$ and $S_2 = \{6\} \times [0,1]$ with a pulsatile pressure type on inlet $-\frac{P_{in}}{2}\left[1 - \cos\left(\frac{\pi t}{2.5}\right)\right]$. With this aim, we have taken the 2D rectangle $\Omega = [0,6] \times [0,1]$, and solved the problem with the Crout method on a structured mesh of 1200 elements, with 2541 nodes P2 for the velocity and 671 nodes P1 for the pressure (Fig. 4.1).

Penerbit Akademia Baru
Journal of Advanced Research in Fluid Mechanics and Thermal Sciences
ISSN (online): 2289-7879 | Vol. 26, No. 1. Pages 1-19, 2016

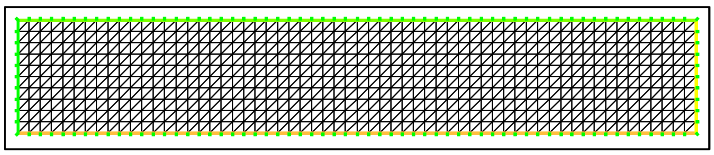

Figure 4.1: Structured mesh employed in a straight pipe.

We take a step time $\Delta t = 0.01\,ms$ and the interval of time [0, 10ms]; a kinematic viscosity $\nu = 1\,poise$ and $P_{in} = 2000 dynes/cm^2$.

The normal velocity increases from the walls until the center, from inlet to outlet (Fig. 4.2 - column at the left) along the pipe, symmetrically relative to the longitudinal axis as a consequence of the propagation of the impulse of the pressure within the pipe. In tangential velocity we can identify an anti-symmetrical behavior with respect to the longitudinal axis of symmetry of the pipe.

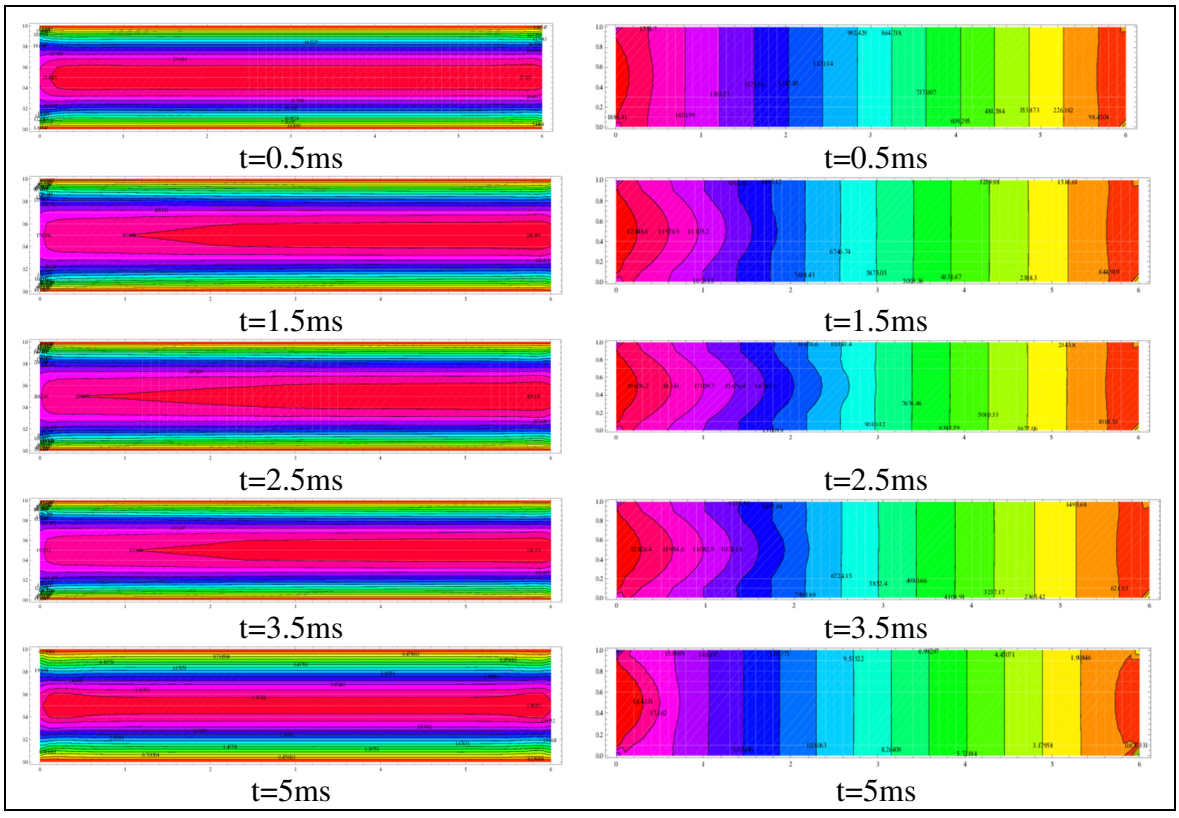

Figure 4.2: Contour plots of normal velocity (on the left) and of pressure (on the right) at different instant of time.

The following plots show the action of each component of velocity over the displacement of the fluid. Both lead the fluid into the center of the pipe and towards the downstream.

Penerbit Akademia Baru
Journal of Advanced Research in Fluid Mechanics and Thermal Sciences
ISSN (online): 2289-7879 | Vol. 26, No. 1. Pages 1-19, 2016

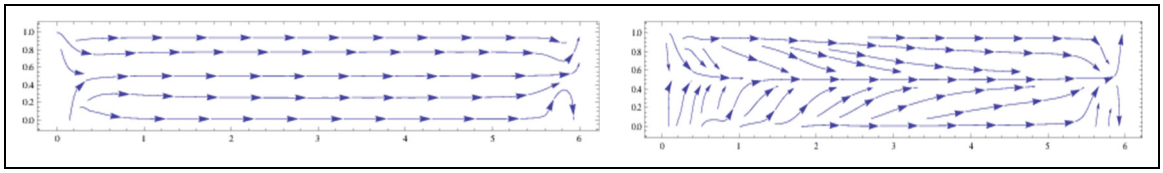

Figure 4.3: The representative vectorial filed of each component of velocity.

These behaviors are visible at any instant of time. However, the maximum magnitude is reached at time t = 2.5ms and t = 7.5ms corresponding to the maximum value of the pressure at the inlet tube, and the minimum value of the magnitude of the normal speed occurs at instant times t = 5ms and t = 10ms, which is when the inlet pressure is zero. In fact, the magnitude of normal velocity has the same sinusoidal behavior of inflow (Fig. 4.4).

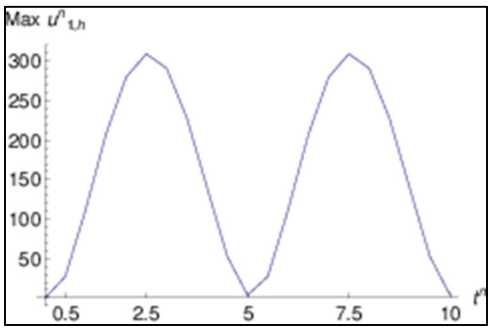

Figure 4.4: Variation of magnitude of the normal velocity in function of time

We can observe a propagation of pressure along the pipe. The increase and decrease of parabolic profile is directly related with the increase and decrease of inlet impulse (Fig. 4.2 - column at the right). The pressure varies on inlet keeping constant over time at the outlet. This means that the wave of inlet impulse is not strong enough to travel until the end of pipe, finishing by dissipate. The whole flow pattern is shown in Fig. 4.5 as instantaneous streamlines and the velocity vector plots. The behavior is the same along the time. We can observe a unidirectional flow laminar type (flow where there is a minimum of agitation of the fluid layers). For each time, we can observe the adjacent streamlines are equally distant which suggests a constant average speed and constant volume flow rate.

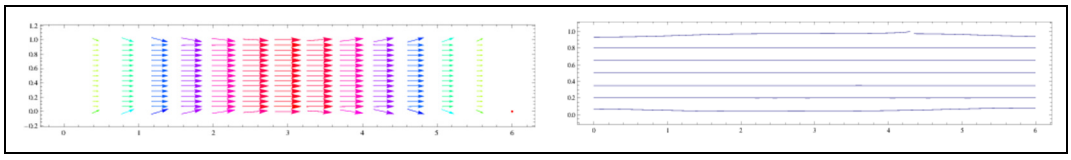

Figure 4.5: The representative vector plot (on the left) and the streamlines (on the right).

To confirm that, we computed the volume flux of fluid crossing a vertical line S_i of the mesh, corresponding to the position $x_i = ih, i = 0,\ldots,60$ and $h = 01cm$, on the axis, i.e.,

$$Q^n(x_i) = \int_{S_i} u_h^n \,.\, n\, dy = \int_{S_i} u_{1,h}^n \,.dy$$

Penerbit Akademia Baru

Journal of Advanced Research in Fluid Mechanics and Thermal Sciences
ISSN (online): 2289-7879 | Vol. 26, No. 1. Pages 1-19, 2016

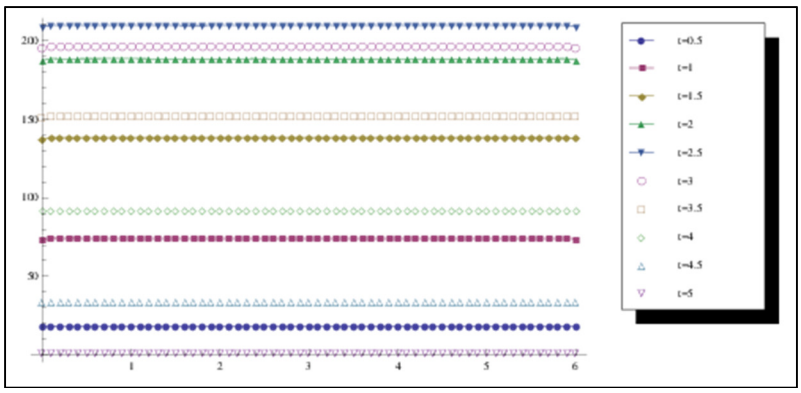

Figure 4.6: The volume flux of fluid at different times

The behavior of velocity and pressure at $t \in [5ms, 10ms]$ repeats comparatively to the qualitative behavior at $t \in [0ms, 5ms]$.

5.0 FLOWS IN A DEFORMED PIPE

5.1 Concave deformation of the upper wall

We take a pipe with a concave deformation of the top wall. We consider the kinematic viscosity $\nu = 1$ and the same time step $t = 0.01ms$. The mesh is unstructured of diameter $h = 10.160605\,\text{cm}$, being $h_{\min} = 0.0554262\,\text{cm}$ the diameter of the smallest element. The mesh is formed by 1948 elements with 1070 nodes P1 and 2679 nodes P2.

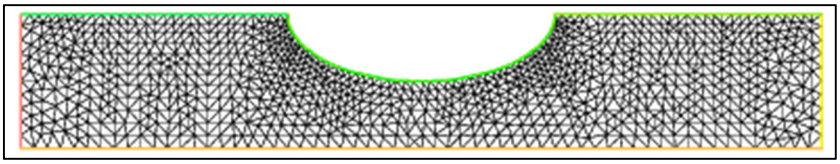

Figure 5.1: Unstructured mesh employed, in a pipe with concave deformation of the upper wall.

The figures below show the normal and tangential velocity (cm/s) at three instants of time significant for their behaviors close to the stenosis.

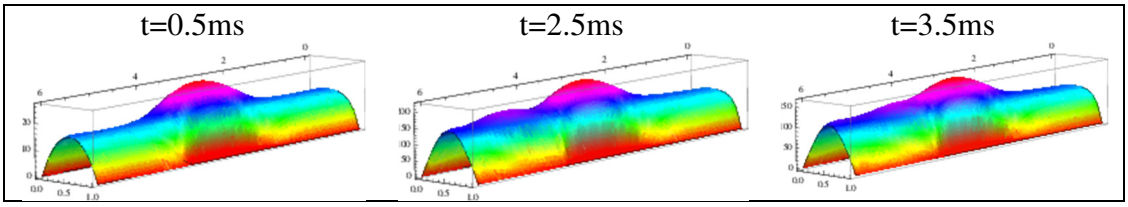

Figure 5.2: Normal velocity at different instants of time, in a pipe with concave deformation of the upper wall.

Penerbit Akademia Baru
Journal of Advanced Research in Fluid Mechanics and Thermal Sciences
ISSN (online): 2289-7879 | Vol. 26, No. 1. Pages 1-19, 2016

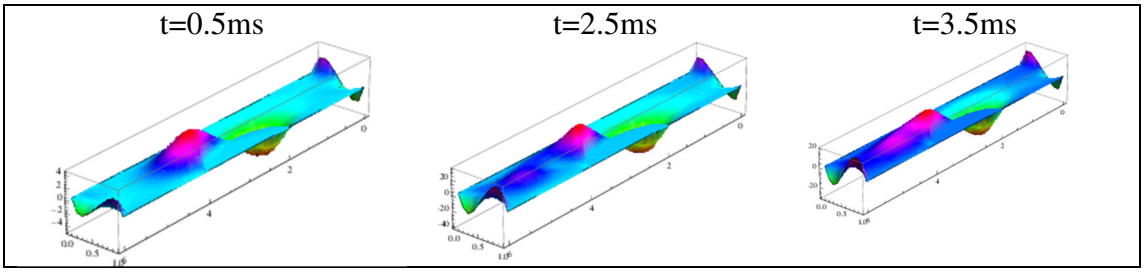

Figure 5.3: Tangential velocity at different instants of time, in a pipe with concave deformation of the upper wall.

We observe that the tangential velocity has an anti-symmetric behavior relatively to the axis of symmetry of stenosis. The minimum values are reached at the first half of the narrowing and the maximum values are reaching in the other half part. The following plots show the action of each component of velocity over the displacement of the fluid. While the normal velocity pushes the fluid against the upper wall slightly towards the downstream, the tangential velocity has the opposite behavior in the first half of the pipe and then reversing their action.

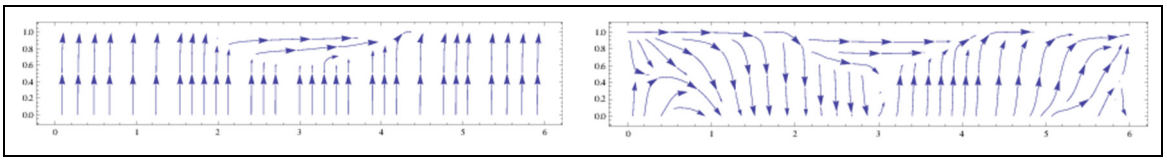

Figure 5.4: The representative vectorial field of each component of velocity, in a pipe with concave deformation of the upper wall.

We notice that the pressure decreases abruptly on stenosis.

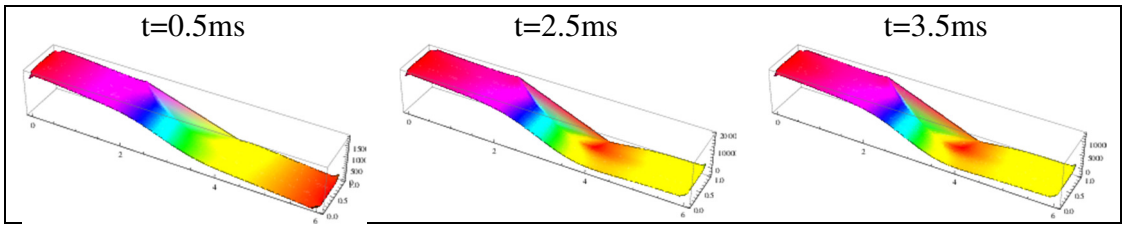

Figure 5.5: Pressure at different instants of time, in a pipe with concave deformation of the upper wall.

We computed the average quantities on each vertical line S_i of the mesh, corresponding to the position $x_i = ih, i = 0,\ldots,60$ and $h = 01cm$, on the axis. In particular, we computed the diameter of the pipe and the averaged pressure at each time:

$$A(x_i) = means(S_i) \qquad \overline{p}^n(x_i) = \frac{1}{A(x_i)} \int_{S_i} p_h^n \; dy$$

The Fig. 5.6 shows the averaged pressure at different instants. It is clear from this plot that the propagating inlet impulse is associated to these quantities.

Penerbit Akademia Baru
Journal of Advanced Research in Fluid Mechanics and Thermal Sciences
ISSN (online): 2289-7879 | Vol. 26, No. 1. Pages 1-19, 2016

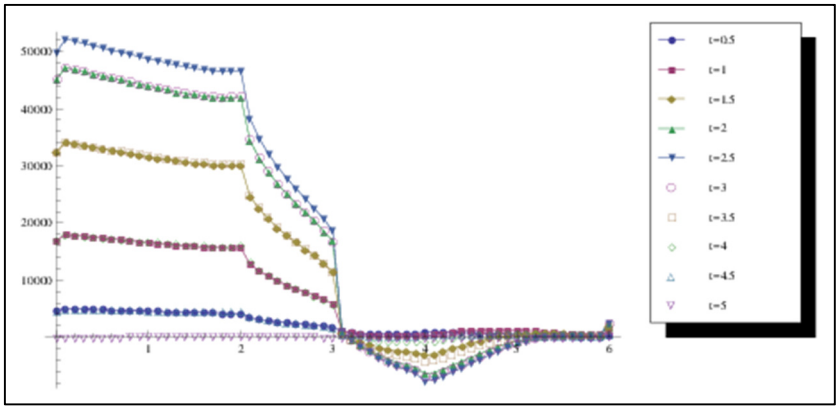

Figure 5.6: The average pressure of fluid $\overline{p}^{n}(x_i)$, at different times, in a pipe with concave deformation of the upper wall.

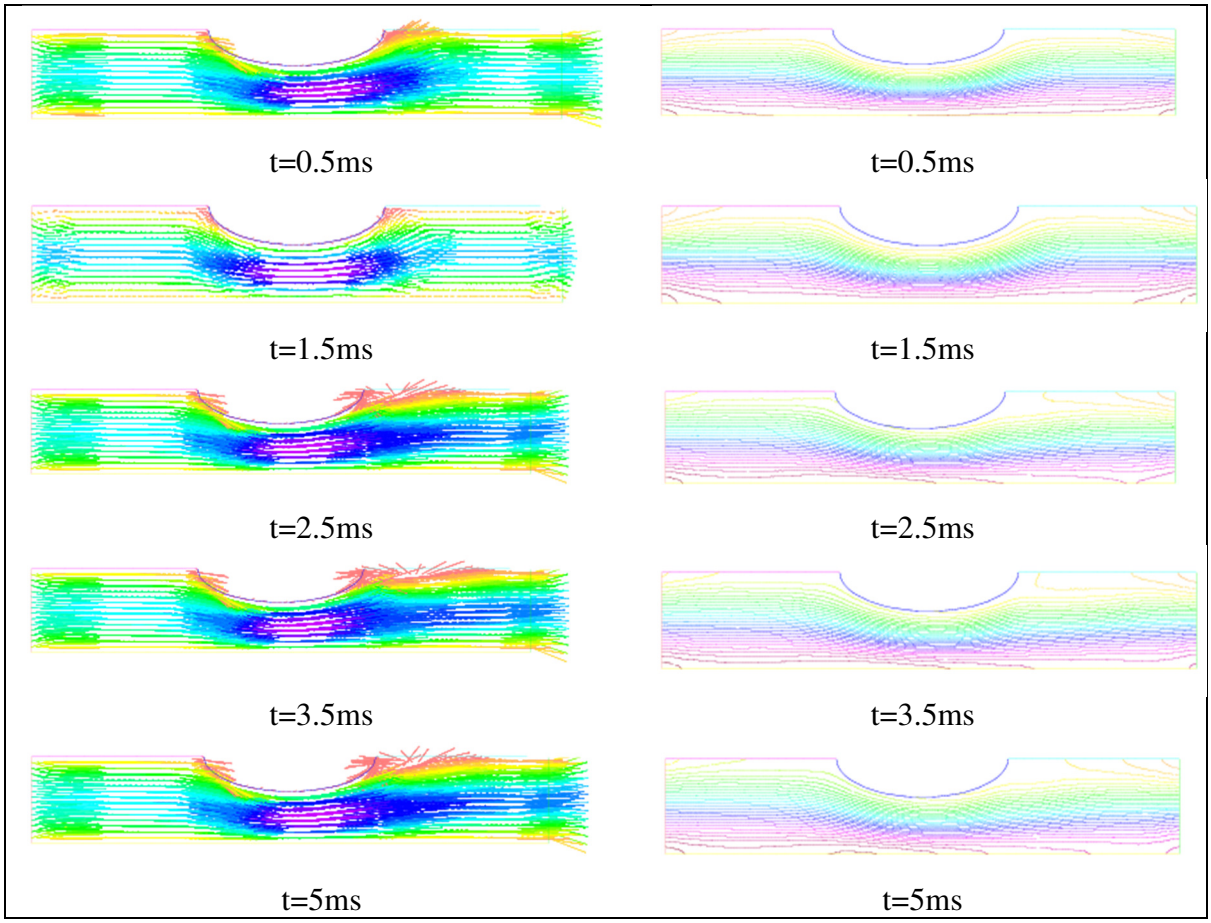

Figure 5.7: The whole flow pattern: velocity vector plots and streamlines at five different times, in a pipe with concave deformation of the upper wall.

Penerbit Akademia Baru
Journal of Advanced Research in Fluid Mechanics and Thermal Sciences
ISSN (online): 2289-7879 | Vol. 26, No. 1. Pages 1-19, 2016

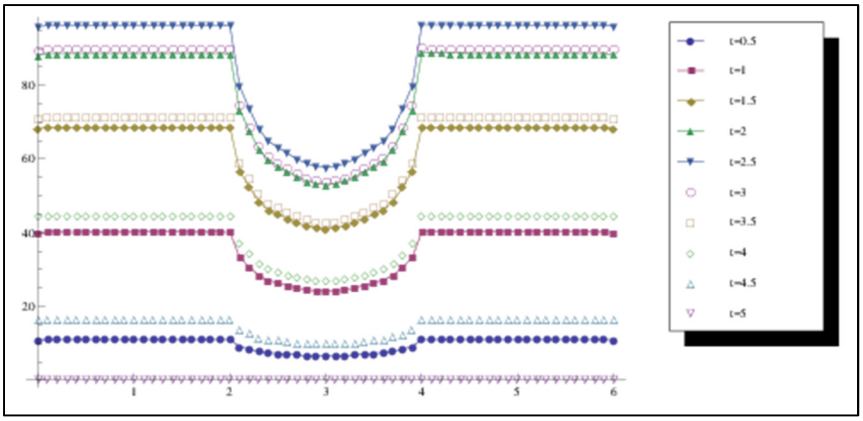

Figure 5.8: The volume flux of fluid $Q^n(x_i)$, at different times, in a pipe with concave deformation of the upper wall.

As in the case of a straight tube the magnitude of the velocity also increases with increase in the input pulse. Values vary significantly with the distance in area of stenosis and also in time during the period of the inlet impulse. It reaches the maximum value in narrowing at the same time as maximum of inlet impulse occurs (see streamlines – Fig. 5.7). The minimum value is reached behind the stenosis. As can be observed in the vector field in the corners of the stenosis exerts some tension, which being much higher at the right where a recirculation arises and it increases with the growth of inlet impulse and decreases as the input pulse reduces. The proximity of streamlines inside the stenosis indicates the increase of average velocity as we refer before and the decrease of volume flux as we can confirm with the Fig. 5.8.

5.2 Convex deformation of the upper wall

We take a pipe with a convex deformation of the top wall. We consider the kinematic viscosity $\nu = 1$ and the same time step $t = 0.01ms$ as before. The mesh is unstructured of diameter $h = 0.153968\,\text{cm}$, being $h_{\min} = 0.0664441\,\text{cm}$ the diameter of the smallest element. The mesh is formed by 1582 elements with 867 nodes P1 and 3315 nodes P2.

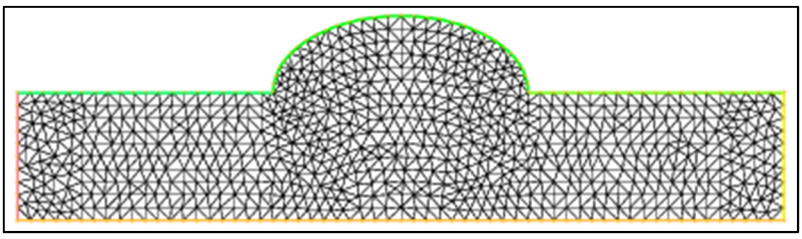

Figure 5.9: Unstructured mesh employed, in a pipe with convex deformation of the upper wall.

Here we observe two distinct flows, one inside the dilatation part and other in the straight pipe. Inside the aneurysm we observed the formation of recirculation of flow. As we can see from the vector plots, there is a big tension on the wall due to the deceleration of the local velocity. This recirculation does not travel out of the bulged region, it remains within the aneurysm. We also observe that this recirculation increases with the inlet impulse and the center of vortex moves to the center of dilation for decreasing its intensity and decreases rapidly the remaining

Penerbit Akademia Baru
Journal of Advanced Research in Fluid Mechanics and Thermal Sciences
ISSN (online): 2289-7879 | Vol. 26, No. 1. Pages 1-19, 2016

inverse flows when the inlet impulse weakens. For other way the flow in the pipe has minimum of agitation. It is laminar type. The magnitude of velocity decreases in pipe in the area of the aneurysm. From the streamlines we observe the waves of inlet impulse. In the zone of dilation, the streamlines are spaced, which allows us to conclude that a decrease average speed and an increasing volume flux in this place, as we can see in Fig. 5.10.

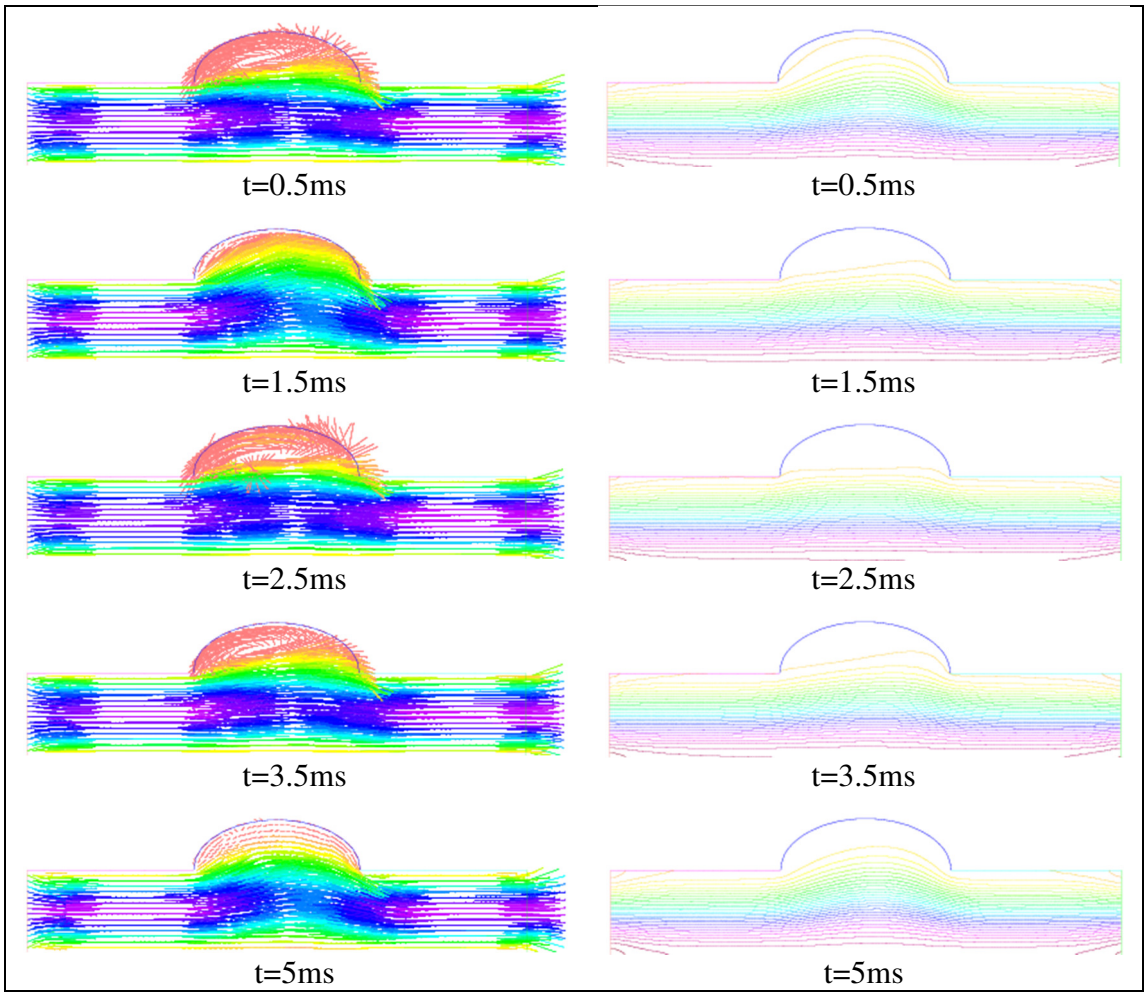

Figure 5.10: The whole flow pattern: velocity vector plots and streamlines at five different times, in a pipe with convex deformation of the upper wall.

The behavior of components of velocity and pressure are qualitatively the same along the time. The normal velocity is lower in the region of dilation. We continue to observe anti-symmetric behavior of the tangential velocity, this time, in relation to the axis of symmetry of zone rounded, assuming the maximum value before of deformation contrary to what happens with the narrowing of the field (deformation concave). The following plots show the action of each component of velocity over the displacement of the fluid. While the normal velocity pushes the fluid against the upper wall.

Penerbit Akademia Baru

Journal of Advanced Research in Fluid Mechanics and Thermal Sciences
ISSN (online): 2289-7879 | Vol. 26, No. 1. Pages 1-19, 2016

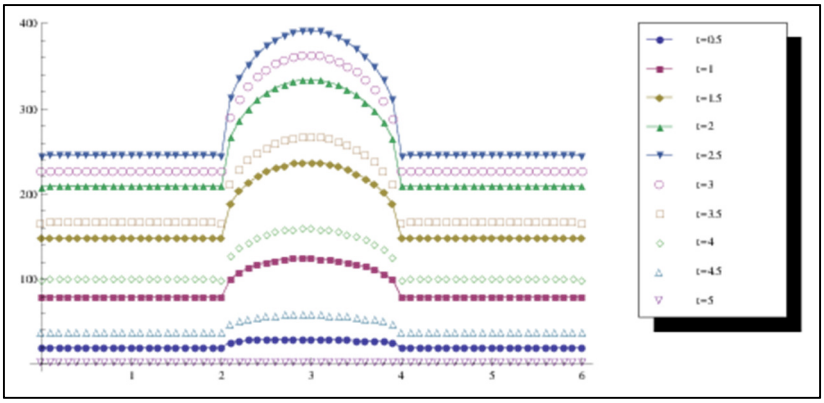

Figure 5.11: The volume flux of fluid $Q^n(x_i)$, at different times, in a pipe with concave deformation of the upper wall.

The figures below show the normal and tangential velocity (cm/s) at three instants of time significant for their behaviors close to the stenosis. The tangential velocity has four distinct actions. First pushes the fluid to the center of the pipe then pushes in the direction of expansion. Within the aneurysm tangential velocity pushes out the fluid after and then it transports down to the outlet. The magnitude of the pressure varies according to the variation of the input pulse, decreasing from upstream to downstream, remaining virtually unchanged at the end of the tube.

We can better verify this behavior taking into account the variation of the average pressure along the tube.

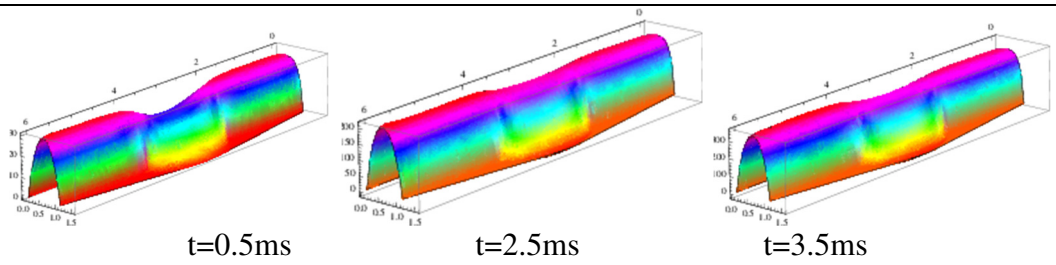

Figure 5.12: Normal velocity at different instants of time, in a pipe with convex deformation of the upper wall.

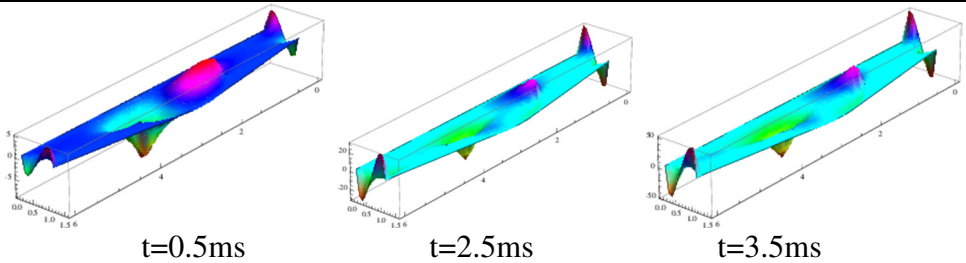

Figure 5.13: Tangential velocity at different instants of time, in a pipe with convex deformation of the upper wall.

Penerbit Akademia Baru

Journal of Advanced Research in Fluid Mechanics and Thermal Sciences
ISSN (online): 2289-7879 | Vol. 26, No. 1. Pages 1-19, 2016

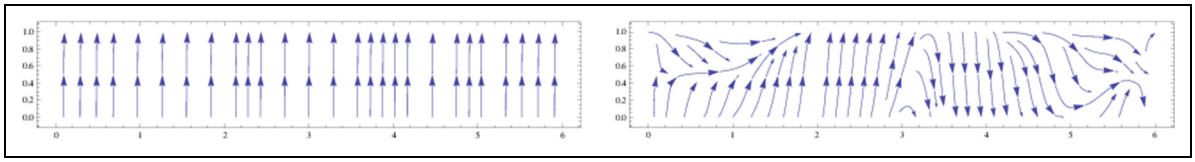

Figure 5.14: The representative vectorial field of each component of velocity, in a pipe with convex deformation of the upper wall.

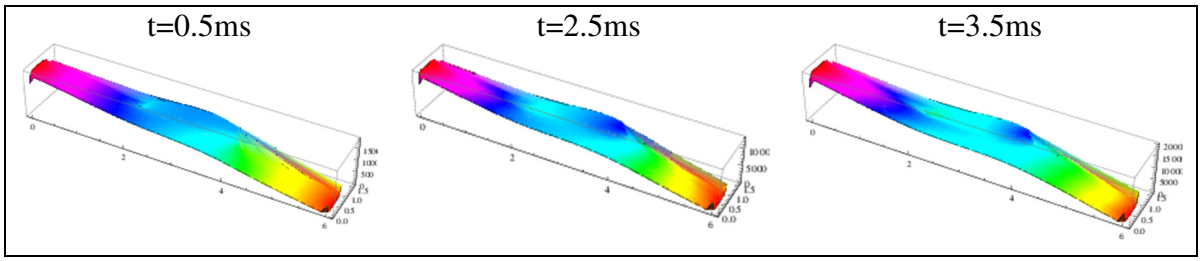

Figure 5.15: Pressure at different instants of time, in a pipe with convex deformation of the upper wall.

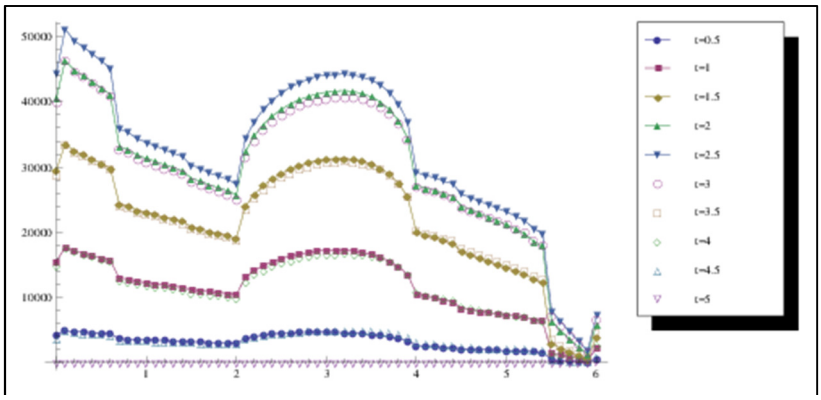

Figure 5.16: The average pressure of fluid $\overline{p}^{n}(x_i)$, at different times, in a pipe with convex deformation of the upper wall.

6.0 DISCUSSION AND CONCLUSIONS

The results of numerical simulations of incompressible Newtonian fluid flows in various geometries is presented and analyzed. Flow behavior of different test cases is investigated an approach of modeling of blood flow and the boundary conditions considered attempted to describe the conditions in the model of blood flow.

By comparing the simulations results from their velocity, velocity vectors, pressure, streamlines and volume flux many differences can be noted due to the geometry of the domain. We observed that for the flow in a deformed pipe with concave deformation the tangential velocity has an anti-symmetric behavior to the axis of stenosis and a recirculation arises at the right which is directly related to the inlet impulse. And for the convex deformation in the upper wall we see the anti-symmetric behavior of tangential velocity in relation to the axis of symmetry of zone rounded and the formation of recirculation of flow takes place inside the aneurysm which remains same within the bulged region.

REFERENCES

[1] Adams, R.A., and Fournier, J.F., Sobolev Spaces, 2nd Edition, Academic Press, NewYork, 2003.

[2] Brenner, Susanne, and Ridgway Scott. The mathematical theory of finite element methods. Vol. 15. Springer Science & Business Media, 2007.

[3] Brezis, Haim. Functional analysis, Sobolev spaces and partial differential equations. Springer Science & Business Media, 2010.

[4] Galdi, Giovanni P. An introduction to the mathematical theory of the Navier-Stokes equations: Steady-state problems. Springer Science & Business Media, 2011.

[5] Raviart, Pierre-Arnaud, and Vivette Girault. Finite element approximation of the navier-stokes equations. Springer Verlag, 1979.

[6] Raviart, Pierre-Arnaud, and Vivette Girault. Finite element approximation of the navier-stokes equations. Springer Verlag, 1979.

[7] F. Hecht, 'FreeFem++', 3rd Edition, Version 3.17, http://www.freefem.org/ff++

[8] Quarteroni, Alfio, and Alberto Valli. Numerical approximation of partial differential equations. Vol. 23. Springer Science & Business Media, 2008.

[9] Temam, Roger. Navier-Stokes equations: theory and numerical analysis. Vol. 343. American Mathematical Soc., 2001.

[10] Rhaman, M. M., and K. M. Helal. "Numerical Simulations of Unsteady Navier-Stokes Equations for Incompressible Newtonian Fluids using FreeFem++ based on Finite Element Method."

[11] Becker, Eric B., Graham F. Carey, and John Tinsley Oden. "Finite Elements, An Introduction: Volume I." 1981.

[12] Shaughnessy, Edward J., Ira M. Katz, and James P. Schaffer. Introduction to fluid mechanics. Vol. 8. New York: Oxford University Press, 2005.

[13] Saad, Y., Iterative Methods for Sparse Linear Systems, 2nd Edition, Society for Industrial and Applied Mathematics, Philadelphia, 2003.

[14] Quarteroni, Alfio, and Luca Formaggia. "Mathematical modelling and numerical simulation of the cardiovascular system." Handbook of numerical analysis 12 (2004): 3-127.

[15] Debnath, Lokenath, and Piotr Mikusiński. Hilbert spaces with applications. Academic press, 2005.

[16] Chorin, Alexandre Joel, Jerrold E. Marsden, and Jerrold E. Marsden. A mathematical introduction to fluid mechanics. Vol. 3. New York: Springer, 1990.

[17] Pal, Madhumangal. Numerical analysis fof scientists and engineers: theory and C programs. 2007.

Journal of Advanced Research in Fluid Mechanics and Thermal Sciences
ISSN (online): 2289-7879 | Vol. 26, No. 1. Pages 1-19, 2016

[18] Ern, Alexandre, and Jean-Luc Guermond. Theory and practice of finite elements. Vol. 159. Springer Science & Business Media, 2013.

[19] Bathe, Klaus-Jürgen. "The inf–sup condition and its evaluation for mixed finite element methods." Computers & structures 79, no. 2 (2001): 243-252.

[20] Hecht, Frédéric. "New development in freefem++." Journal of Numerical Mathematics 20, no. 3-4 (2012): 251-266.

[21] Wong, M.K., Sheng, L.C., Nor Azwadi, C.S., Hashim, G.A., "Numerical Study of Turbulent Flow in Pipe with Sudden Expansion" Journal of Advanced Research in Fluid Mechanics and Thermal Sciences 6 (2015).

[22] Sapee, S. "Computational Fluid Dynamics Study on Droplet Size of Kerosene Fuel" Journal of Advanced Research in Fluid Mechanics and Thermal Sciences 16 (2015).